

Document downloaded from:

<http://hdl.handle.net/10251/176487>

This paper must be cited as:

Cecilia, J.; Soriano Rodríguez, MD.; Marques Correia, L.; Rodríguez-Castellón, E.; López Nieto, JM.; Silveira Vieira, R. (2020). Fe<sub>2</sub>O<sub>3</sub> supported on hollow micro/mesospheres silica for the catalytic partial oxidation of H<sub>2</sub>S to sulfur. *Microporous and Mesoporous Materials*. 294:1-10. <https://doi.org/10.1016/j.micromeso.2019.109875>



The final publication is available at

<https://doi.org/10.1016/j.micromeso.2019.109875>

Copyright Elsevier

Additional Information

# **Fe<sub>2</sub>O<sub>3</sub> supported on hollow micro/mesospheres silica for the catalytic partial oxidation of H<sub>2</sub>S to Sulfur**

By

J.A. Cecilia<sup>1,\*</sup>, M.D. Soriano<sup>2</sup>, L. Marques-Correia<sup>3</sup>, E. Rodríguez-Castellón<sup>1</sup>, J.M. López Nieto<sup>2</sup>, R. Silveira-Vieira<sup>3</sup>

<sup>1</sup> Departamento de Química Inorgánica, Cristalografía y Mineralogía, Facultad de Ciencias, Universidad de Málaga, 29071 Málaga, Spain.

<sup>2</sup> Instituto de Tecnología Química, Universitat Politècnica de València-Consejo Superior de Investigaciones Científicas, 46022 Valencia, Spain.

<sup>3</sup> Grupo de Pesquisa em Separações por Adsorção (GPSA), Departamento de Engenharia Química, Universidade Federal do Ceará, Campus do Pici, Bl. 709, 60.455-760 Fortaleza-CE, Brazil.

\*Email: [jacecilia@uma.es](mailto:jacecilia@uma.es)

## **Abstract**

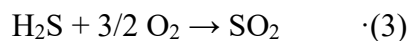
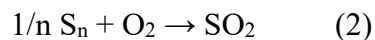
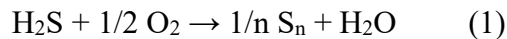
A family of Fe-based catalysts supported on hollow silica mesospheres have been synthesized and tested in the catalytic partial oxidation of H<sub>2</sub>S to elemental sulfur at 170-180°C, atmospheric pressure and under 300 minutes of time-on-stream. The characterization of the synthesized catalysts by X-ray diffraction (XRD), scanning electron microscopy (SEM), transmission electron microscopy (TEM), diffuse reflectance UV-vis spectra (DRS), H<sub>2</sub>-temperature programmed reduction (H<sub>2</sub>-TPR), N<sub>2</sub> adsorption-desorption at -196 °C and X-ray photoelectron spectroscopy (XPS) reveals the formation of a catalytic system with high micro- and mesoporosity and high dispersion of the Fe<sub>2</sub>O<sub>3</sub> species. The catalytic results reported a high activity in the partial oxidation of H<sub>2</sub>S, reaching over the HMS-10Fe (i.e. with 10 wt% of iron loading) catalyst at 180 °C and after 300 minutes of time in the stream (TOS), a higher conversion value close to 94% with a selectivity towards elemental sulfur of 98%. The comparison of HMS-10Fe catalysts with other SiO<sub>2</sub>-based supports, as a fumed silica (Cab-osil; Cab) or a mesoporous silica (SBA-15), indicates changes in the catalytic activity for H<sub>2</sub>S conversion depending on support, and showing the following trend: HMS-10Fe > SBA-10Fe > Cab-10Fe. These results suggest that the use of a support with a narrow pore tend to achieve facilitate the iron dispersion favoring higher conversion rates.

**Keywords:** Fe<sub>2</sub>O<sub>3</sub>, H<sub>2</sub>S, selective oxidation, elemental sulfur, hollow silica mesospheres

## 1. Introduction

The removal of H<sub>2</sub>S is a challenge extremely important from different point of view, as environmental, economic and public health. Environmental regulations have been developed to modulate the maximum H<sub>2</sub>S release rates allowed to the atmosphere, as well its presence in industrial gases. Moreover, H<sub>2</sub>S, either gas and/or solution, is extremely corrosive to piping and production facilities [1]. Occupational Safety and Health Administration (OSHA) has reported that a concentration of 100 ppm of H<sub>2</sub>S is considered to be immediately dangerous to life and health (IDLH) [2]. Since H<sub>2</sub>S occurs in crude petroleum, natural gas, and hot springs, the main activities in which occupational exposure is likely are petroleum and natural gas drilling, refining, and coke ovens [3,4]. Additionally, since hydrogen sulfide is formed during the decay of organic matter, wastewater treatment plants, landfills, and tanneries are also important emitting sources [5]. Finally, the Kraft process employed in many paper mills, which involves using sodium hydroxide and sodium sulfide also results in the emission of H<sub>2</sub>S.

The Claus process patented by Carl Friedrich Claus in 1883 in England is the most used process for oxidation of H<sub>2</sub>S to elemental sulfur, using typically Fe and Al<sub>2</sub>O<sub>3</sub> as catalysts, in a temperature range of 400 °C to 600 °C. However, this process has thermodynamic limitations and low sulfur conversion and 3-5% of the H<sub>2</sub>S cannot be converted to elemental sulfur [6]. The most advanced technology to removal the H<sub>2</sub>S content is the selective oxidation of H<sub>2</sub>S to elemental sulfur, which is based on the irreversible selective oxidation of H<sub>2</sub>S to sulfur (reaction (1)) as the main reaction, with other oxidation reactions (reactions (2) and (3)) and the reversible Claus reaction (reaction (4)) as side reactions.



In this sense, both Mobil direct oxidation process (MODOP) and the Super Claus process treat the tail gases obtained after the Claus process on other sources more benign

environmentally. In the case of the MODOP process, H<sub>2</sub>S is partially oxidized to elemental sulfur using a stoichiometric amount of oxygen and TiO<sub>2</sub> as catalyst. The main disadvantage of this process is related with the formation of H<sub>2</sub>O as by-product, which must be removed since it causes the deactivation of the catalyst [7]. In the Super-Claus process, the dehydration step does not occur so the catalyst used in these processes are more resistant to deactivation processes, although it is required an excess of oxygen to obtain high sulfur yields [8].

The catalysts used in the partial oxidation of H<sub>2</sub>S reaction must present a controlled oxidative capacity, since the use of catalysts with a high oxidative activity can lead to the formation of undesirable product in the reaction, such as SO<sub>2</sub>, an environmental contaminant with high toxicity [9,10].

In the last years, several metal oxides have been studied as the active phase in the selective oxidation H<sub>2</sub>S reaction for elemental sulfur formation. The catalysts most studied are: V<sub>2</sub>O<sub>5</sub>, Mn<sub>2</sub>O<sub>3</sub>, Fe<sub>2</sub>O<sub>3</sub>, CuO, NiO, CoO and Bi<sub>2</sub>O<sub>3</sub> [11-15]. In this sense, isotopical studies have reported that metal oxides are partially reduced under the reaction medium forming MO<sub>2</sub><sup>-</sup> species, which leads to MOS<sup>-</sup> and then MS<sub>2</sub><sup>-</sup> species by the following reaction exchange (reactions 5 and 6) [15].



It has been reported in the literature that the V<sub>2</sub>O<sub>5</sub>-based catalysts have been highly studied due to its high activity and selectivity towards elemental sulfur. It has been reported in the literature that its catalytic activity is ascribed to the partial reduction of the V<sub>2</sub>O<sub>5</sub> phase to V<sub>4</sub>O<sub>9</sub>, which displays the V<sup>5+</sup>-O-V<sup>4+</sup> pairs that are active in the partial oxidation of H<sub>2</sub>S to elemental sulfur, and decreasing the combustion of elemental sulfur to SO<sub>2</sub> [16,17].

Nowadays, the scientific community is searching and developing more competitive process to be implanted in industrial scale. Fe-based catalysts have emerged a potential catalyst in oxidation reactions, such as methane oxidation [18] or volatile organic compounds (VOCs) [19]. In the case of the partial oxidation of H<sub>2</sub>S to elemental sulfur, the Fe<sub>2</sub>O<sub>3</sub>-based catalysts are more inexpensive materials than V<sub>2</sub>O<sub>5</sub>-based catalysts,

attaining high conversion values. However, the main drawback of the Fe<sub>2</sub>O<sub>3</sub>-based catalysts is related with its low selectivity towards elemental sulfur, resulting in high proportions of undesired SO<sub>2</sub> (which is formed mainly by combustion of elemental sulfur) [20,21]. However, it has been reported that the selectivity to elemental sulfur can be improved if the size of the Fe<sub>2</sub>O<sub>3</sub> crystals are small and these crystals are dispersed in an appropriate support [10,22].

It has been reported in the literature that the adsorption of H<sub>2</sub>S takes place by the interaction between S atom of H<sub>2</sub>S adsorption on the top site of Fe atom, being H<sub>2</sub>S- $\alpha$ -Fe<sub>2</sub>O<sub>3</sub> (001), the most stable configuration. After H<sub>2</sub>S adsorption, a sequential dissociation process of H<sub>2</sub>S occurs with giving rise to surface HS, S, H species via reactions of H<sub>2</sub>S  $\rightarrow$  H + HS and HS  $\rightarrow$  H + S on  $\alpha$ -Fe<sub>2</sub>O<sub>3</sub>(001) surface [23].

Considering these premises, several authors have evaluated different Fe.-based catalytic system, such as Fe<sub>2</sub>O<sub>3</sub>/SiO<sub>2</sub> [22,24], Fe<sub>2</sub>O<sub>3</sub>/Al<sub>2</sub>O<sub>3</sub> [25,26], Fe<sub>2</sub>O<sub>3</sub>/MgO [27], Fe<sub>2</sub>O<sub>3</sub>/CeO<sub>2</sub> [28], Fe<sub>2</sub>O<sub>3</sub>/TiO<sub>2</sub> [29], Fe<sub>2</sub>O<sub>3</sub>/Al-PILC [30], Fe<sub>2</sub>O<sub>3</sub>/SiC [31-33], iron-antimonate (FeSbO<sub>4</sub>) catalysts [34], iron-molybdate (Fe<sub>2</sub>(MoO<sub>4</sub>)<sub>3</sub>) catalysts [35] in the partial oxidation of H<sub>2</sub>S to elemental sulfur.

In this sense, Terörde et al. evaluated the catalytic activity of the Fe<sub>2</sub>O<sub>3</sub> using several oxides as support [36]. These authors established the following trend: Fe<sub>2</sub>O<sub>3</sub>/SiO<sub>2</sub> > Fe<sub>2</sub>O<sub>3</sub>/TiO<sub>2</sub> > Fe<sub>2</sub>O<sub>3</sub>/ZrO<sub>2</sub> > Fe<sub>2</sub>O<sub>3</sub>/Al<sub>2</sub>O<sub>3</sub> >> Fe<sub>2</sub>O<sub>3</sub>/MgO due to the interaction between the active phase and the support as well as the weak acidity of the SiO<sub>2</sub> used as support. In addition, they pointed out that the increase of the reaction temperature is directly related with the catalytic conversion, improving the selectivity toward elemental sulfur and diminishing the levels towards undesired SO<sub>2</sub> species.

The aim of the present research is the synthesis of hollow silica mesospheres, which will be used as support with high specific surface area, high thermochemical stability and homogeneous pore width to disperse small particles of Fe<sub>2</sub>O<sub>3</sub>, which has shown to be highly active in the selective oxidation of H<sub>2</sub>S to elemental sulfur in the literature, although not always highly selective towards elemental sulfur.

## 2. Experimental

## 2.1. Reagents

The chemicals used to synthesize the HMS were dodecylamine (Merck, 98%), tetraethyl orthosilicate (Aldrich, 98%) and ethanol (VWR, 96%). The aqueous solutions were prepared using ultrapure water of type 1 (Milli-Q) with resistivity less than ( $18.2 \text{ M}\Omega\text{cm}^{-1}$ ) at 25 °C. The iron oxide source was iron nitrate nonahydrated (Aldrich, 98%). The gases were He (Air Liquide 99.99 %), N<sub>2</sub> (Air Liquide 99.9999 %), H<sub>2</sub>/Ar (10% vol. in H<sub>2</sub>, Air Liquide 99.99 %) and H<sub>2</sub>S/He 1% vol. in H<sub>2</sub>S, Linde 99.99 %).

## 2.2. Synthesis of the catalysts

HMS were synthesis according the methodology proposed by Cecilia et al. [37]. In this present research, HMS was synthesized using a non-ionic template route (S<sup>0</sup>I<sup>0</sup>), which tends to form porous materials with higher surface area and greater wall thickness. This fact supposes the synthesis of porous frameworks with higher thermal and mechanical stability in comporation to those HMS synthesized using cationic surfactant (S<sup>+</sup>I) [38].

In a typical synthesis of HMS, 27 mL of ethanol and 32.5 mL of ultrapure water was mixed with 4.65 g of n-docecyamine, used as neutral surfactant. This solution was stirred for 30 min and then, 17.5 mL TEOS (as silica source) were added. This solution was maintained at 25 °C for 24h. The molar final composition of the synthesis gel formed was 0.025n-dodecylamine/1.850 H<sub>2</sub>O/0.462EtOH/0.078TEOS. The obtained solid was filtered, water washed and dried at 60 °C for 12 h. The dried solid was calcined at 550 °C, using a heating rate of 1 °C/min, and maintained at this temperature for 6 h.

The iron oxide (Fe<sub>2</sub>O<sub>3</sub>) species were incorporated using, Fe(NO<sub>3</sub>)<sub>3</sub>·9H<sub>2</sub>O as iron source, by the incipient wetness method and dried at 60 °C overnight. Finally, all the samples were calcined at 400 °C for 4 h under air flow. The samples were labeled as HMS-xFe, where x is refers to the iron loading (in wt.%) on the support in a range of 2.5–20 wt.%.

## 2.3. Catalyst characterization

Powder patterns for the samples were collected on an X'Pert Pro MPD automated diffractometer (PANalytical B.V) equipped with a Ge (111) primary monochromator

(strictly monochromatic Cu  $K\alpha_1$  radiation) and an X'Celerator detector. The diffractograms were determined in the range of  $2\theta$  of 1-10° and 10-70° with step size of 0.017° in 30 min. Crystalline phases were identified by matching experimental patterns to the JCPDS powder diffraction file.

The morphology of HMS was determined by scanning electron microscopy (SEM). The pieces were goldcoated in a JEOL Ion Sputter JFC-1100 device for about 10 min (goldcoat w300A thick). The morphology of the HMS-xFe catalysts was also studied by transmission electron microscopy (TEM), by using a FEI Talos F200X equipment, which combines outstanding high-resolution S/TEM and TEM imaging with energy dispersive x-ray spectroscopy (EDS) signal detection, and 3D chemical characterization with compositional mapping.

Diffuse reflectance UV-vis spectra (DRS) were collected on a Cary 5 apparatus equipped with a 'Praying Mantis' attachment (from Harric) under ambient conditions.

The H<sub>2</sub>-TPR experiments were performed with the catalyst precursor (0.080 g), previously treated with a He flow (35 mL min<sup>-1</sup>) at 100 °C for 45 min. After the sample cooled to room temperature, the H<sub>2</sub> consumption was studied between 50 and 800 °C in an Ar/H<sub>2</sub> flow (48 mL min<sup>-1</sup>, 10 vol% of H<sub>2</sub>) at a heating rate of 10 °C min<sup>-1</sup>. The water formed in the reduction reaction was trapped by passing the exit flow through a cold finger immersed in a liquid N<sub>2</sub>/isopropyl alcohol bath (-80 °C). The H<sub>2</sub> registration was performed with a thermal conductivity detector (TCD).

The textural properties were evaluated from the N<sub>2</sub> adsorption-desorption isotherms at -196 °C, as determined by an automatic ASAP 2020 system from Micromeritics. Prior the measurements, the samples were outgassed overnight at 200 °C and 10<sup>-4</sup> mbar. The surface areas were determined with the BET equation and a N<sub>2</sub> cross-section of 16.2 Å<sup>2</sup>. The total pore volume was calculated from the adsorption isotherm at  $P/P_0=0.996$ . The DFT method was employed to determine the pore-size distributions.

X-ray photoelectron spectra were collected using a Physical Electronics PHI 5700 spectrometer with non-monochromatic MgK $\alpha$  radiation (300 W, 15 kV, and 1253.6 eV) with a multi-channel detector. Spectra of pelletized samples were recorded in the constant pass energy mode at 29.35 eV, using a 720  $\mu$ m diameter analysis area. Charge

referencing was measured against adventitious carbon (C 1s at 284.8 eV). A PHI ACCESS ESCA-V6.0 F software package was used for acquisition and data analysis. A Shirley-type background was subtracted from the signals. Recorded spectra were always fitted using Gaussian–Lorentzian curves in order to determine the binding energies of the different element core levels more accurately.

Elemental analysis was performed to determine the sulfur content, in the used catalyst, using a LECO CNHS 932 elemental analysis apparatus.

#### 2.4. Catalytic tests

Catalytic experiments for partial oxidation of H<sub>2</sub>S to S were performed in a fixed-bed quartz tubular flow reactor, operating at atmospheric pressure at two different reaction temperatures (i.e. 170 °C and 180 °C). The analysis of the feed composition of the reagents and products for the reaction were identified and quantified by gas chromatography equipped with TCD detector and two chromatographic columns (Molecular Sieve 5A and Porapak T). The reaction conditions used were 100 mg of catalyst (particle size 40-60 mesh), operating with a total flow rate of 130 mL min<sup>-1</sup> and a molar ratio H<sub>2</sub>S/Air/He of the 1.2/5/93.8. Equations 4, 5 and 6, define as the conversion of H<sub>2</sub>S (wt. %), S selectivity (wt. %) and SO<sub>2</sub> selectivity (wt. %) were calculated:

$$H_2S \text{ conversion} = \frac{(H_2S)_{in} - (H_2S)_{out}}{(H_2S)_{in}} \times 100 \quad (4)$$

$$\text{Sulfur selectivity (wt. \%)} = \frac{(H_2S)_{in} - (H_2S)_{out} - (SO_2)_{out}}{(H_2S)_{in} - (H_2S)_{out}} \times 100 \quad (5)$$

$$SO_2 \text{ selectivity (wt. \%)} = \frac{(SO_2)_{out}}{(H_2S)_{in} - (H_2S)_{out}} \times 100 \quad (6)$$

where: (H<sub>2</sub>S)<sub>in</sub> and (H<sub>2</sub>S)<sub>out</sub>, respectively, are the initial and final concentrations of H<sub>2</sub>S and (SO<sub>2</sub>)<sub>out</sub> is the final concentration of SO<sub>2</sub>, which may be formed in the partial selective oxidation reaction of H<sub>2</sub>S. In our case, the reaction mixture that leaves the reactor is cooled, collecting sulfur (which is weighed after each experiment). The resulting mixture (without sulfur) is passed through the chromatographic column to analyze N<sub>2</sub>, O<sub>2</sub> and SO<sub>2</sub>.

### 3. Results and discussion

#### 3.1. Catalyst characterization

The high range ordering of the HMS was determined by low angle X-ray diffraction (Figure 1A). Its diffractogram displays a broad band located between  $2\theta = 1.5$ - $3.0^\circ$ , which is ascribed to the (100) reflection and another band with lower intensity, ascribed to the overlapping of the (110) and (200) reflections. This profile is similar to that obtained for another porous silica, as MCM-41 [39].

The XRD of the iron-based catalysts (Figure 1B) show a broad band located around  $2\theta = 23^\circ$ , which can be attributed to the walls of mesoporous silica ( $\text{SiO}_2$ ) [40,41]. In no case, it is observed other diffraction peaks, indicating that the iron-species are amorphous or displays a crystalline domains are too small to be detected with this technique. The absence of diffraction peaks ascribed to iron species also was confirmed when other porous materials, such as SBA-15 [22] or porous clay heterostructures [42] were used as support. However, when using  $\text{SiO}_2$  as support, it has been reported the presence of diffraction peaks ascribed to the formation of hematite ( $\alpha\text{-Fe}_2\text{O}_3$ ) crystals [42], so it is expected that the mesoporous supports must disperse the small  $\text{Fe}_2\text{O}_3$  crystals.

The morphology of the hollow silica mesospheres was determined by scanning electron microscopy (SEM) and transmission electron microscopy (TEM). Both SEM and TEM images (Figure 2) show the agglomeration of pseudo-spherical particles with a size around 300-400 nm. On the other hand, the compositional mapping of the HMS- $x\text{Fe}$  catalysts (Figure 3), determined by EDAX, also confirms the high dispersion of the Fe-species, even for the catalysts with higher Fe-content, as was suggested from the XRD data (Figure 1B).

As the iron oxide species were not detected by XRD in any catalyst, diffuse reflectance UV-Vis spectra have been recorded in order to discern the characteristics of the iron species (Figure 4). The profiles of the UV-Vis spectra reveals how the decrease of the bands are shifted to higher wavelength due to the increase in Fe-content generates an increment in coloring. The UV-Vis hardly show different between. However, it is noticeable the coexistence of two Fe-entities in all catalysts [43]

Figure 5 compiles the H<sub>2</sub>-TPR experiments of the HMS-*x*Fe catalysts. In all cases, it can be observed a broad band, between 220 and 550 °C, attributed to overlapping several reduction steps of the Fe-species (Fe<sub>2</sub>O<sub>3</sub> → Fe<sub>3</sub>O<sub>4</sub> → FeO → Fe<sup>0</sup>) so it is difficult discern each reduction step [42,44]. Several authors have pointed out the coexistence of two or even three reduction step. These authors have indicated that the differences between the H<sub>2</sub>-TPR profiles are attributed to different stabilization of FeO<sub>*x*</sub> species due to a higher or lower interaction between the FeO<sub>*x*</sub> species and the support [45-47]. In the present research, the reduction the Fe-species takes place at a relatively low temperature, which supposes a low interaction of the Fe<sub>2</sub>O<sub>3</sub> particles with the support as well as the existence of small Fe<sub>2</sub>O<sub>3</sub> particles, as was suggested from XRD and TEM data (Figure 1B and 3). Nonetheless, it is noteworthy a slight shift of the H<sub>2</sub>-TPR profile at lower reduction temperature when the Fe-content increase in the catalysts. This fact could indicate that the catalysts with lower Fe-contents display a stronger interaction with the support than those catalysts with higher Fe-content. Finally, the absence of bands at higher temperature (>550 °C) discards the formation of quasi-bulk Fe<sub>2</sub>O<sub>3</sub>-species and/or the incorporation of Fe-species into the SiO<sub>2</sub> framework.

The textural properties of the HMS-*x*Fe catalysts was determined by N<sub>2</sub> adsorption-desorption at -196 °C (Figure 6A). According to the IUPAC classification, both the support and HMS-*x*Fe catalysts displays IVb-type isotherm, which is typical of mesoporous structures [48]. The absence of hysteresis loops is attributed to porous structures with a pore size lower than 4 nm [48]. The specific surface area, determined from the BET equation (Table 1), shows how the HMS display a high S<sub>BET</sub> value (1093 m<sup>2</sup> g<sup>-1</sup>). The high value of the *t*-plot data (877 m<sup>2</sup> g<sup>-1</sup>) reveals that this support is mainly microporous, as suggested the absence of hysteresis loop in the adsorption isotherm. The high microporosity of the SiO<sub>2</sub>-particles confirms that these spherical structures can be considered as hollow. The incorporation of Fe-species by incipient wetness impregnation and subsequent calcination causes a progressive decay of the S<sub>BET</sub> and the *t*-plot values probably due to the Fe-species are partially blocking the entry of the mesoporous channels. In any case, the catalysts still maintain high micro- and mesoporosity since the catalyst with highest Fe-content (HMS-20Fe) displays a S<sub>BET</sub> value of 792 m<sup>2</sup> g<sup>-1</sup>.

The analysis of the pore volume (Table 1) follows the same to that observed for the specific surface area since the HMS material has a pore volume of  $0.940 \text{ cm}^3 \text{ g}^{-1}$ . As was indicated previously, the pore volume is mainly ascribed to the high microporosity ( $V_p$  plot:  $0.719 \text{ cm}^3 \text{ g}^{-1}$ ). In the same way, the pore volume decreases as higher content is incorporated.

The pore size distribution was determined by DFT calculations (Figure 6B). In the case of the HMS, it can be observed on one hand the presence of micropores with a pore width between 1.3-1.6 nm and on the other hand the existence of small mesopores with a maximum pore width of 3.0 nm. As was suggested from the adsorption isotherms, the incorporation of Fe-species causes a progressive loss of the micro- and mesoporosity.

In order to determine the superficial chemical composition of the HMS-xFe catalysts, XPS measurements were carried out. Fe  $2p$  core level spectra (Figure 7) show similar profiles for all catalysts since all of them display a contribution located at 710.4-710.7 eV, which is ascribed to the existence of  $\text{Fe}^{3+}$  species in the form of  $\text{Fe}_2\text{O}_3$  or  $\text{FeOOH}$  [42,49]. With regard to the O  $1s$  core level spectra, it is also observed a contribution located about 532.7-532.8 eV, that is assigned to the presence of oxides species [49]. In the case of the Si  $2p$  core level spectra, the unique contribution, located at 102.8 eV, is assigned to the silica species of the support [49].

The atomic concentration on the surface of the HMS-xFe catalysts, compiled in Table 2, reveals that the Fe-content on the surface increases directly with the wt.% incorporated in the impregnation step. The analysis of the Fe-; content on the surface (in wt.%) determined by XPS is close to the theoretical value for the catalyst with lower Fe-content; however, these values move away from the theoretical value as the Fe-content increases. These values can be related to the  $\text{H}_2$ -TPR profiles (Figure 5) since catalysts with low iron content have a greater dispersion on their surface so the  $\text{Fe}_2\text{O}_3$ -support interaction must be greater than those catalysts with higher Fe content where the Fe particles seem to be overlapped between them in such a way there is a lower interaction of the support.

### *3.2. Catalytic performance*

The HMS-*x*Fe catalysts were tested in the partial oxidation of H<sub>2</sub>S to elemental sulfur, following the experimental conditions described above. The reactants and reaction products (i.e. O<sub>2</sub>, H<sub>2</sub>S, H<sub>2</sub>O and SO<sub>2</sub>) achieved at 170 °C during 300 min of time on stream, were monitored by gas chromatography. In order to evaluate the catalytic behavior of the Fe-sites, and taking into account the high dispersion of the active phase in all HMS-*x*Fe catalysts, the catalytic activity was indicated from H<sub>2</sub>S converted per hour and per gram of Fe (Figure 8A). These data shows that the Fe-sites are most active and efficiency for the HMS-*x*Fe catalysts with lower Fe-content (HMS-2.5Fe), attaining an initial H<sub>2</sub>S conversion of 1.39 mol h<sup>-1</sup> g<sub>Fe</sub><sup>-1</sup>. However, the catalytic activity is diminished below its half (0.75 mol h<sup>-1</sup> g<sub>Fe</sub><sup>-1</sup>) after 300 min of TOS. An increase of the Fe content leads to Fe-sites with lower efficiency, although with lower catalyst decay suggesting that the active sites in these catalysts sites are less susceptible to deactivation processes along the TOS.

With regard to the distribution of reaction products (Figure 8B-C), it can be concluded that elemental sulfur is the main reaction product, with a selectivity above 95% at 170 °C and after 300 min of TOS, while the undesired SO<sub>2</sub> is below 5% in all catalysts. No apparent changes in the selectivity to sulfur were observed after 300 min of time on stream. In this sense, previous research have reported that Fe-catalysts are highly active in the selective oxidation of H<sub>2</sub>S reaction, although the Fe<sub>2</sub>O<sub>3</sub>-phase tends to favor the formation of combustion product, i.e. SO<sub>2</sub> [20,21]. The decrease of the Fe<sub>2</sub>O<sub>3</sub>-crystals causes an increases of the number of the available Fe-sites and favors the partial reduction of the Fe<sub>2</sub>O<sub>3</sub>-crystals at lower temperature under the reaction medium, forming MOS<sup>-</sup> and then MS<sub>2</sub><sup>-</sup> species, as indicated the reactions 5 and 6 [15], and then the subsequent desorption of the sulfur species as elemental sulfur [23], which is in agreement with that reported in the present research since small Fe<sub>2</sub>O<sub>3</sub> crystals are highly active in the selective oxidation of H<sub>2</sub>S to elemental sulfur.

In order to understand the catalytic process and assess the evolution of the active phase, the HMS-*x*Fe catalysts were collected after 300 min of TOS at 170 °C and then they were studied by XPS. The analysis of the Fe 2*p* core level spectra for the used catalysts does not show modification in comparison to their respective fresh catalysts (Table 2). This fact suggests that Fe-species should not undergo drastic changes in its chemical composition during the reaction. On the other hand, it is noteworthy the

appearance of new signals in the S 2*p* region after the reaction (Figure 9A). All spectra display a main contribution located between 163.2-163.4 eV, which is assigned to elemental sulfur and another much less intense band, located between 168.0-168.2 eV, that are attributed to SO<sub>2</sub>-species. These data are in agreement with the catalytic data (Figure 8B-C), since the main product is elemental sulfur in all cases, while the content of the undesired SO<sub>2</sub> is negligible. The analysis of the atomic concentrations, compiled in Table 2, shows how the sulfur content on the surface increases slightly for the catalysts higher Fe-content. This fact can be in concordance with the higher proportion of Fe-species on the surface, which favors the selective adsorption of the H<sub>2</sub>S by the Fe<sub>2</sub>O<sub>3</sub> sites, as was reported in previous research [15,23], and it suggests the decrease of the superficial Fe/Si molar ratio after the catalytic tests. In addition, the partial blockage of the micro- and mesopores (Table 1) by the incorporation of the Fe<sub>2</sub>O<sub>3</sub> species can also favor that the H<sub>2</sub>S partial oxidation may be favored on the surface of the catalyst, causing an increase of the sulfur content, as reveals the XPS studies. In any case, the high sulfur content in the form of elemental sulfur indicates that these species are strongly adsorbed under these reaction conditions. This fact progressively blocks the amount of available active sites for the partial selective oxidation reaction of H<sub>2</sub>S, causing a gradual deactivation along the TOS.

The use of lower reaction temperature allows to save energy in industrial scale processes. However, the elemental sulfur obtained as product in this reaction can be condensed in the micropores, leading to diffusional limitations as well as a decrease of the available active sites [8]. Therefore, it is necessary the use of higher reaction temperature to remove the chemisorbed sulfide, although this increase must be controlled since it can lead to the formation of undesired products such as SO<sub>2</sub> [20,21]. Thus, a slight increase in the reaction temperature, from 170 °C to 180 °C, reports a greater resistance to the deactivation of catalyst, mainly for long reaction times, as shows Figure 10. When comparing H<sub>2</sub>S conversions (Figure 10A), it can be observed how HMS-2.5Fe catalyst is more active at 170 °C for shorter reaction times probably because the chemisorption H<sub>2</sub>S- $\alpha$ -Fe<sub>2</sub>O<sub>3</sub> is favored at lower reaction temperature [23]; however, the H<sub>2</sub>S conversion is higher for a reaction temperature of 180 °C after 120 min (suggesting a lower catalyst decay). This fact is more pronounced for the HMS-10Fe catalyst since

the use of a reaction temperature of 170 °C causes a strong deactivation after only 60 min of TOS, reaching a FUR conversion close to 59% after 300 min of TOS, while the increase of the reaction temperature, only 10 °C more, barely causes deactivation processes, attaining a H<sub>2</sub>S conversion of 94% after 300 min at 180 °C. With regards to the selectivity (Figure 10B-C), the slight increase of the temperature hardly modifies the selectivity pattern, being elemental sulfur the main product. Both HMS-2.5Fe and HMS-10Fe catalysts display a slight increase of the SO<sub>2</sub> selectivity from about 2 % at 170 °C to 6% for the HMS-2.5Fe catalyst and 9% for the HMS-10Fe at 180 °C after the first minutes of TOS.

Both HMS-2.5Fe and HMS-10Fe catalysts after the reaction at 180 °C during 300 min were also studied by XPS (Figure 9B). S 2*p* core level spectra of both used catalysts maintain those two contributions shown at lower reaction temperature, being the contribution attributed to SO<sub>2</sub> species negligible. In addition, it is also noteworthy that the sulfur content on the surface of both catalysts are lower than those shown for lower reaction temperature since the superficial sulfur decrease from 3.84% to 1.21% in the case of the HMS-2.5Fe catalyst and from 3.33% to 3.01% for the HMS-10Fe catalyst when the reaction temperature only rises 10 °C. This fact implies a lower proportion of sulfur deposits that are blocking the Fe<sub>2</sub>O<sub>3</sub> sites and a less pronounced deactivation along the TOS, as was reported in Figure 10A.

Finally, the HMS-10Fe catalyst was compared with other Fe-based catalysts supported on other silicas with different framework, as a fumed silica (Cab-osil) formed by solid spheres with a diameter between 0.2-0.3 μm and a SBA-15, which possesses parallel with a homogeneous pore width around 5 nm. As takes place for HMS-10Fe, SBA-10Fe does not display any diffraction peaks (Figure 11), which suggests a high dispersion of the Fe-species. However, Cab-10Fe displays diffraction peaks located at  $2\theta$  (°) = 33.1, 35.6, 40.8, 49.4, 53.9, 62.4 and 63.9 that are assigned to the presence of Fe<sub>2</sub>O<sub>3</sub> species. The presence of these diffraction peaks suggests that Cab-10Fe catalyst presents bigger Fe<sub>2</sub>O<sub>3</sub> crystals than the other Fe-based catalysts supported on other silicas. In the same way, the analysis of the atomic concentrations, estimated from the XPS spectra, reveals that Cab-10Fe catalyst display the lowest concentration of Fe on its surface, since

the Fe content is only 2.41%. This data is agreement with bigger Fe<sub>2</sub>O<sub>3</sub> crystal size and subsequent lower dispersion of the active phase on the surface of the support.

The textural properties of the Fe-based catalysts supported on different silicas are compiled in Table 1. The comparison between all Fe-based catalysts reveals that the catalyst supported in HMS is the one that presents a higher specific surface area ( $S_{\text{BET}}$ ), being mainly a microporous catalyst, as indicates its high  $t$ -plot value and its micropore volume. In the opposite case, the Fe-catalyst supported on the commercial silica (Cab-10Fe) presents the lowest  $S_{\text{BET}}$  value, only 161 m<sup>2</sup> g<sup>-1</sup>. In addition, this catalyst is eminently macroporous since the commercial silica is formed by solid microspheres so its surface area and pore volume are attributed to its interparticular voids. In the case of the SBA-10Fe sample, the catalyst is mainly mesoporous, although it is also noteworthy a proportion of microporosity by the interconnection of meso-channels.

The comparison between all Fe-based catalysts supported on different silicas shows how HMS-10Fe sample is the most active catalyst in the selective oxidation of H<sub>2</sub>S to elemental sulfur (Figure 12A), maintaining a H<sub>2</sub>S conversion close to 94% after 300 min of TOS at 180 °C. In the case of the SBA-10Fe, the conversion is almost total during the first 60 min of TOS; however, this catalyst is more susceptible to deactivation reaching a H<sub>2</sub>S conversion of 65% after 300 min of TOS at 180 °C. Taking into account that both catalyst present its active phase well-dispersed, the greater tendency to the catalytic deactivation that presents the SBA-10Fe catalyst in comparison to the HMS-10Fe catalyst could be attributed to difference between the textural properties of both catalysts. Thus, the higher microporosity of the HMS-10Fe catalyst can favor a more intimate contact between a small molecule, as H<sub>2</sub>S, with the Fe<sub>2</sub>O<sub>3</sub> sites. In contrast, the increase of the pore diameter in the SBA-10Fe catalyst limits the interaction between the H<sub>2</sub>S molecules and the Fe<sub>2</sub>O<sub>3</sub>-sites, since the H<sub>2</sub>S molecules are small and the support is not modulated to such a small target molecule so the interaction with the active sites must be lower having an adverse effect on the catalytic behavior. The catalytic deactivation is more pronounced in the case of the Cab-10Fe catalyst, attaining a H<sub>2</sub>S conversion of 53% after 300 min of TOS at 180 °C, due to a decrease in the number of active centers available by the formation of bigger Fe<sub>2</sub>O<sub>3</sub> crystals (Figure 11) as well as the use of a

support with higher pore size, which further limits the contact of the H<sub>2</sub>S molecules and the Fe<sub>2</sub>O<sub>3</sub>-sites and its catalytic activity.

With regard to the selectivity (Figure 12B-C), elemental sulfur is the main product for all catalysts, although SBA-10Fe and mainly HMS-10Fe are the most selective ones, which reaches a selectivity above 96% after 300 min of TOS at 180 °C. In the case of the Cab-10Fe, the selectivity towards elemental sulfur decrease, obtaining higher proportions of undesired SO<sub>2</sub>, since its selectivity is above 37% after 300 min of TOS at 180 °C. This data is in agreement with the literature where previous authors have reported that the formation of bigger Fe<sub>2</sub>O<sub>3</sub> crystals tends to give rise to SO<sub>2</sub> as a majority product [20-22].

#### **4. Conclusion**

A series of HMS-*x*Fe catalysts have been synthesized and then were evaluated in the selective oxidation of H<sub>2</sub>S to elemental sulfur. The characterization of these catalysts reveals a high dispersion of the Fe<sub>2</sub>O<sub>3</sub>-species supported on hollow silica mesospheres with homogeneous pore size, about 3 nm and high surface area.

The catalytic results revealed that the HMS-*x*Fe catalysts are highly active in the selective oxidation of H<sub>2</sub>S, obtaining an almost total selectivity towards elemental sulfur. However, these catalysts are susceptible to deactivation processes at long reaction times by the strong adsorption of the obtained products on the surface of catalyst, blocking the available Fe-sites. The increase of the reaction temperature minimizes the deactivation process, leading to more stable catalyst. Nevertheless, this increase of the temperature must be controlled since it can modify the selectivities pattern, obtaining higher values of SO<sub>2</sub>.

The morphology of the support also plays a key role in the catalytic behavior. The catalytic results suggest that the use of a porous material with small pore diameter favors the interaction between a small molecule as H<sub>2</sub>S with the active phase (Fe<sub>2</sub>O<sub>3</sub>), although this narrow pore size distribution can also cause a blockage of the micro- and mesochannels and a faster deactivation by the deposition of elemental sulfur.

## **Acknowledgements**

The authors wish to acknowledge the financial support provided by projects RTI2018-099668-B-C21 and RTI2018-099668-B-C22 of Ministerio de Ciencia, Innovación y Universidades, and project UMA18-FEDERJA-126 of Junta de Andalucía and FEDER funds. In addition, the authors also thank Fundação Cearense de Apoio ao Desenvolvimento Científico e Tecnológico (FUNCAP) by the Coordenação de Aperfeiçoamento de Pessoal de Nível Superior (CAPES) - Processo: PDSE 99999.002602/2014-08.

## References

- [1] V. Garcia-Arriaga, J. Alvarez-Ramirez, M. Amaya, E. Sosa, *Corros. Sci.* 52 (2010) 2268-2279.
- [2] Occupational Safety and Health Administration, USA, OSHA Standards: Hydrogen sulfide exposure. Available online:  
<https://www.osha.gov/SLTC/hydrogensulfide/standards.html>
- [3] K.H. Kim, Y.J. Choi, E.C. Jeon, Y. Sunwoo, *Atmos. Environ.* 39 (2005) 1103-1112.
- [4] K.H. Kim, E.C. Jeon, Y.J. Choi, Y.S. Koo, *Atmos. Environ.* 40 (2006) 4478-4490.
- [5] L. Zhang, P. De Schryver, B. De Gussemme, W. De Muynck, N. Boon, W. Verstraete, *Water Res.* 42 (2008) 1-12.
- [6] B.G. Goar, *Oil Gas J.* 34 (1975) 96-98.
- [7] R. Kettner, N. Liermann, *Oil Gas J.* 11 (1982) 63-66.
- [8] P.F.M.T. van Nisselrooy, J.A. Lagas, *Catal. Today* 16 (1993) 263-271.
- [9] A. Piéplu, O. Saur, J-C. Lavalley, C. Nédez, *Catal. Rev.- Sci. Eng.* 40 (1998) 409-450.
- [10] X. Zhang, Y. Tang, J. Da, H. Zhengping, *ACS Catal.* 5 (2015) 1053-1067.
- [11] P.J. Van den Brink, R.J.A.M. Terörde, J.H. Moors, A.J. Van Dillen, J.W. Geus, *Stud. Surf. Sci. Catal.* 72 (1992) 123-132.
- [12] K-T. Li, W-Da. Cheng, *Appl. Catal. A* 142 (1996) 315-326.
- [13] A.A. Davydov, V.I. Marshneva, M.L. Shepotko, *Appl. Catal. Catal. A* 244 (2003) 93-100.
- [14] S. Yasyerli, *Chem. Eng. Process.* 47 (2008) 577-584.
- [15] M.Y. Jia, X.L. Ding, S.G. He, M.F. Ge, *J. Phys. Chem. A* 117 (2013) 8377-8387.
- [16] M.D. Soriano, J. Jiménez-Jiménez, P. Concepción, A. Jiménez-López, E. Rodríguez-Castellón, J.M. López Nieto, *Appl. Catal. B* 92 (2009) 271-279.

- [17] M.D. Soriano, J.A. Cecilia, A. Natoli, J. Jiménez-Jiménez, J.M. López Nieto, E. Rodríguez-Castellón, *Catal. Today* 254 (2015) 36-42.
- [18] V.A. Sazonov, Z.R. Ismagilov, N.A. Prokudina, *Catal. Today* 47 (1999) 149-153.
- [19] B. Solsona, T. García, R. Sanchis, M.D. Soriano, M. Moreno, E. Rodríguez-Castellón, S. Agouram, A. Dejoz, J.M. López Nieto, *Chem. Eng. J.* 290 (2016) 273-281.
- [20] J.H. Uhm, M.Y. Shin, J. Zhidong, J.S. Chung, *Appl. Catal. B* 22 (1999) 293-303.
- [21] E. Laperdrix, G. Costentin, N. Nguyen, F. Studer, J.C. Lavalley, *Catal. Today*. 61 (2000) 149-155.
- [22] A. Reyes-Carmona, M.D. Soriano, J.M. López Nieto, D.J. Jones, J. Jiménez-Jiménez, A. Jiménez-López, E. Rodríguez-Castellón, *Catal. Today* 210 (2013) 117-123.
- [23] J. Song, X. Niu, L. Ling, B. Wang, *Fuel Process. Technol.* 115 (2013) 26-33.
- [24] G.A. Bukhtiyarova, V.I. Bukhtiyarov, N.S. Sakaeva, V.V. Kaichev, B.P. Zolotovskii, *Appl. Catal. A* 158 (2000) 251-255.
- [25] E.K. Lee, K.D. Jung, O.S. Joo, Y.G. Shul, *Appl. Catal. A* 239 (2005) 64-67.
- [26] M.A. Shields, N.L. Dowling, P.D. Clark, *Ind. Eng. Chem. Res.* 48 (2007) 7721-7728.
- [27] K.D. Jung, O.S. Joo, C.S. Kim, *Catal. Lett.* 84 (2002) 1-2.
- [28] D.D.E. Koyuncu, S. Yasyerli, *Ind. Eng. Chem. Res.* 48 (2009) 5223-5229.
- [29] H. M. Tadesmir, S. Yasyerli, N. Yasyerli, *Int. J. Hydrogen Energy.* 40 (2015) 9980-10001.
- [30] X. Zhang, D. Guangyu, Z. Wang, L. Li, Y. Wang, H. Wang, *J. Hazard. Mater.* 260 (2013) 104-111.
- [31] N. Keller, C. Pham-Huu, M.J. Ledoux, *Appl. Catal., A.* 217 (2001) 205-217.
- [32] P. Nguyen, D. Edouard, J.M. Nhut, M.J. Ledoux, Ch. Pham, C. Pham-Huu, *Appl. Catal. A.* 76 (2007) 300-310.
- [33] P. Nguyen, J.M. Nhut, D. Edouard, C. Pham, M.J. Ledoux, C. Pham-Huu, *Catal. Today.* 141 (2009) 397-402.

- [34] K.T. Li, C.S. Yen, N.S. Shyu, *Appl. Catal. A* 156 (1997) 117-130.
- [35] U. Kersen, R.L. Keiski, *Catal. Commun.* 10 (2009) 1039-1042.
- [36] R.J.A.M. Terorde, P.J. van den Brink, L.M. Visser, A.J. van Dillen, J.W. Geus, *Catal. Today* 17 (1993) 217-223.
- [37] J.A. Cecilia, E. Vilarrasa-García, C. García-Sancho, R.M.A. Saboya, D.C.S. Azevedo, C.L. Cavalcante Jr., E. Rodríguez-Castellón, *Int. J. Greenhouse Gas Control* 52 (2016) 344-356.
- [38] P.T. Tanev, T.J. Pinnavaia, *Science* 267 (1995) 865-867).
- [39] U. Ciesla, F. Schüth, *Micropor. Mesopor. Mater.* 27 (1999) 131-149.
- [40] J. Zhang, Z. Tong, *J. Nat. Prod. Gas Chem.* 15 (2006) 63-69.
- [41] W. Gac, A. Derylo-Marczewska, S. Pasieczna-Patkowska, N. Popivnyah, G. Zukocinski, *J. Mol. Catal. A: Chem* 1 (2007) 15-23.
- [42] R. Sanchis, J.A. Cecilia, M.D. Soriano, M.I. Vázquez, A. Dejoz, J.M. López Nieto, E. Rodríguez Castellón, B. Solsona, *Chem. Eng. J.* 334 (2018) 1159-1168
- [43] L. Luo, C. Dai, A. Zhang, J. Wang, Ch Song, X. Guo, *RSC Adv.* 6 (2016) 32789-32797.
- [44] J.A. Pena, E. Lorente, E. Romero, J. Herguido, *Catal. Today* 116 (2006) 439-444.
- [45] K. Park, J.H. Jung, H. Seo, O. Kwon, *Microp. Mesop. Mat.* 121 (2009) 219-225.
- [46] F.G.E. Nogueira, J.H. Lopes, A.C. Silva, R.M. Lago, J.D. Fabris, L.C.A. Oliveira, *Appl. Clay Sci.* 51 (2011) 385-389.
- [47] H. Hayashi, M. Kishida, K. Wakabayashi, *Catal. Surv. Jpn.* 6 (2002) 9-17.
- [48] M. Thommes, K. Kaneko, A.V. Neimark, J.P. Olivier, F. Rodriguez-Reinoso, J. Rouquerol, K.S.W. Sing, *Pure Appl. Chem.* 87 (2015) 1051-1069.
- [49] J.F. Moulder, W.F. Stickle, P.E. Sobol, K.D. Bomben, *Handbook of X-ray Photoelectron Spectroscopy*, Perkin-Elmer Corp, Eden Prairie, MN, 1992.

**Table 1.** Textural parameters of the Fe containing mesoporous silica materials.

<b>Sample</b>	<b>S<sub>BET</sub></b> <b>(m<sup>2</sup>g<sup>-1</sup>)</b>	<b>t-plot</b> <b>(m<sup>2</sup>g<sup>-1</sup>)</b>	<b>V<sub>P</sub></b> <b>(cm<sup>3</sup> g<sup>-1</sup>)</b>	<b>V<sub>MICROP</sub></b> <b>(cm<sup>3</sup> g<sup>-1</sup>)</b>
<b>HMS</b>	1093	877	0.940	0.719
<b>HMS-2.5Fe</b>	1022	770	0.885	0.636
<b>HMS-5Fe</b>	989	720	0.830	0.572
<b>HMS-10Fe</b>	924	714	0.731	0.520
<b>HMS-15Fe</b>	872	698	0.643	0.466
<b>HMS-20Fe</b>	792	672	0.565	0.430
<b>SBA-10Fe</b>	523	233	0.342	0.104
<b>Cab-10Fe</b>	161	22	0.568	0.019

**Table 2.** Surface composition of the HMS-xFe catalysts determined by XPS.

Catalyst	Atomic Concentration (%)				Molar ratio		
	C	Si	O	Fe	S	Fe/Si	Fe/S
HMS-2.5Fe	8.00	26.47	64.70	0.83 (2.39)	-	0.031	-
HMS-2.5Fe-u	3.02	26.43	65.99	0.72 (2.00)	3.84	0.027	0.188
HMS-5Fe	5.39	27.51	66.07	1.03 (2.92)	-	0.037	-
HMS-5Fe-u	2.89	27.09	65.28	0.77 (2.14)	3.97	0.028	0.194
HMS-10Fe	3.39	27.72	67.63	1.26 (3.55)	-	0.045	-
HMS-10Fe-u	6.21	25.18	64.48	0.80 (2.29)	3.33	0.032	0.240
HMS-15Fe	9.58	25.37	63.40	1.64 (4.77)	-	0.065	-
HMS-15Fe-u	4.13	24.47	64.89	1.44 (3.97)	5.05	0.059	0.285
HMS-20Fe	5.52	27.07	65.93	1.67 (4.71)	-	0.062	-
HMS-20Fe-u	3.93	24.14	64.65	1.45 (3.96)	6.42	0.060	0.226

## Captions to Figures

**Figure 1.** Low-angle x-ray diffraction of the HMS (A) and high-angle x-ray diffractions (B) of the HMS and HMS-xFe catalysts.

**Figure 2.** SEM (A) and TEM (B) images of the HMS.

**Figure 3.** S/TEM images and compositional mapping of HMS-2.5Fe, HMS-10Fe and HMS-20Fe catalysts.

**Figure 4.** Diffuse reflectance UV–vis of the HMS-xFe catalysts.

**Figure 5.** H<sub>2</sub>-TPR of the HMS-xFe catalysts.

**Figure 6.** N<sub>2</sub>-adsorption isotherms (A) and pore size distribution (estimated by DFT method) of the HMS-xFe catalysts.

**Figure 7.** Fe 2*p* core level spectra of the HMS-xFe catalysts.

**Figure 8.** H<sub>2</sub>S converted (A), elemental sulfur (B) and SO<sub>2</sub> obtained (C) in the selective oxidation of H<sub>2</sub>S to elemental sulfur. Catalytic conditions: 0.1 g of catalyst; total flow of 130 mL min<sup>-1</sup>; 300 min of TOS; reaction temperature of 170 °C; H<sub>2</sub>S/air/He molar ratio of 1.2/5.0/93.8.

**Figure 9.** S 2*p* core level spectra of the HMS-xFe catalysts after the selective H<sub>2</sub>S oxidation. Catalytic conditions: 0.1 g of catalyst; total flow of 130 mL min<sup>-1</sup>; 300 min of TOS; reaction temperature of 170 C; H<sub>2</sub>S/air/He molar ratio of 1.2/5.0/93.8 (A). S 2*p* core level spectra of HMS-2.5Fe and HMS-10Fe catalysts after the selective H<sub>2</sub>S. Catalytic conditions: 0.1 g of catalyst; total flow of 130 mL min<sup>-1</sup>; 300 min of TOS; reaction temperature of 170-180 °C; H<sub>2</sub>S/air/He molar ratio of 1.2/5.0/93.8 (B).

**Figure 10.** H<sub>2</sub>S converted (A), elemental sulfur (B) and SO<sub>2</sub> obtained (C) in the selective oxidation of H<sub>2</sub>S to elemental sulfur. Catalytic conditions: 0.1 g of catalyst; total flow of 130 mL min<sup>-1</sup>; 300 min of TOS; reaction temperature of 170-180 °C; H<sub>2</sub>S/air/He molar ratio of 1.2/5.0/93.8.

**Figure 11.** X-ray diffractions of Fe-based catalysts supported on different silicas.

**Figure 12.** H<sub>2</sub>S converted (A), elemental sulfur (B) and SO<sub>2</sub> obtained (C) in the selective oxidation of H<sub>2</sub>S to elemental sulfur for the Fe-based catalysts supported on different silicas. Catalytic conditions: 0.1 g of catalyst; total flow of 130 mL min<sup>-1</sup>; 300 min of TOS; reaction temperature of 180 °C; H<sub>2</sub>S/air/He molar ratio of 1.2/5.0/93.8.

